Inorganic Chemistry

Article

pubs.acs.org/IC

Symmetry-Related $[Ln^{III}_6Mn^{III}_{12}]$ Clusters toward Single-Molecule Magnets and Cryogenic Magnetic Refrigerants

Jun-Liang Liu, Wei-Quan Lin, Yan-Cong Chen, Ji-Dong Leng, Fu-Sheng Guo, and Ming-Liang Tong*

MOE Key Lab of Bioinorganic and Synthetic Chemistry, State Key Laboratory of Optoelectronic Materials and Technologies, School of Chemistry & Chemical Engineering, Sun Yat-Sen University, Guangzhou 510275, People's Republic of China

Supporting Information

ABSTRACT: A family of high-nuclearity $[Ln^{III}_6Mn^{III}_{12}]$ (Ln = Gd, Tb) nanomagnets has been synthesized, of which two are in D_2 molecular symmetry and the other two are in C_1 symmetry. X-ray crystallography shows that each of them contains a similar $\{Mn^{III}_8O_{13}\}$ unit, four marginal Mn^{III} ions, and two linear $\{Ln^{III}_3\}$ units with parallel or perpendicular orientation for high- and low-symmetry cores, respectively. For $[Gd^{III}_6Mn^{III}_{12}]$, the distinct spins of the $\{Mn^{III}_8O_{13}\}$ unit lead to different spin ground states (S_T = 23 for the high-symmetry one and S_T = 16 for the low-symmetry one), and significant magnetocaloric effects are observed in a wide temperature range [full width at half-maximum (FWHM) of $-\Delta S_m$ > 18 K] that can maximizes the refrigerant capacity, which may be attributed to the ferromagnetic interactions. By replacement of isotropic Gd^{III} with anisotropic Tb^{III}, they behave as single-molecule magnets, with the high-symmetry one possessing a larger effective barrier (36.6 K) than the low-symmetry one (19.6 K).

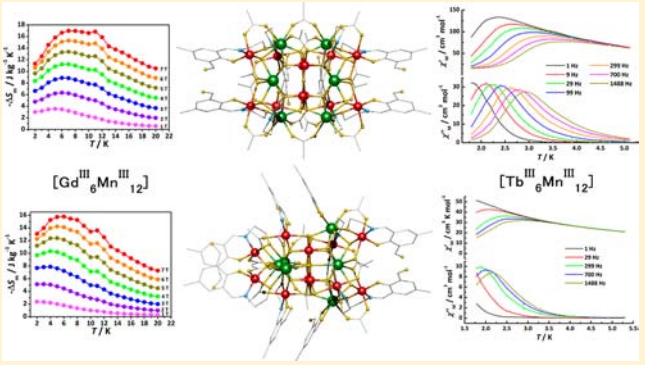

INTRODUCTION

Nanomagnets of high-nuclearity metal clusters are some of the attractive fields of synthetic chemistry and molecular magnetism for their aesthetically pleasing structures with interesting magnetic properties, as well as play a role in understanding the interplay between the macroscale classical properties and microscale quantum properties.[1−4] Some of these families exhibit very high ground-state spin, even up to $S = {}^{83}/_{2}$;[5] thus, they are favorable as significant molecular magnetic refrigerants[4,6,7] and well-performed single-molecule magnets (SMMs).[7−9]

A refrigerator based on vapor-cycle technology is widely used in our daily life and academic research. In the last century, the cryogenic magnetocaloric effect (MCE) was discovered and succeeded in reaching ultralow temperatures via a process known as adiabatic demagnetization.[4,10] Thus, Giauque received the 1949 Nobel Prize in Chemistry. Nowadays, adiabatic demagnetization with the magnetic refrigerant is one of the promising technologies for obtaining ultralow temperatures, even in the milliKelvin temperature range.[11] Compared with traditional technology, adiabatic demagnetization is energy-saving and environmentally friendly, emits little noise, and easily achieves ultralow temperature. Among magnetic refrigerants, molecule-based magnets can avoid the decline of magnetic entropy changes ($-\Delta S_m$) that arise by long-range order, compared with traditional alloys.[4,6,7]

In the pursuit of the well-performed magnetic refrigerants, the factors of (1) spins per unit of weight, (2) magnetic anisotropy, and (3) spin degeneracy are all of importance.[4,6,7] Of course, the level population of spin multiplets cannot be negligible. Isotropic and weak magnetic coupling clusters lead to the presence of low-lying excited states and can maximize the magnetic entropy changes, but actually, no matter how weak the interaction is, it is unavoidable that the magnetic exchange removes the degeneracy and further splits the energy levels of spin multiplets, influencing the behavior of MCE to some extent. As the proverb goes, *there ain't no such thing as a free lunch*. The role of ferromagnetic interaction acts like a double-edged sword: though it removes the degeneracy of the energy levels and lowers the zero-field magnetic entropy, it provides a route to rapidly increase the magnetic entropy on demagnetization, leading to a large MCE in a wide temperature range, especially at high temperature and under small field.

High-spin ground state (S_T) is also believed to be one of the important factors for regulating the effective barrier of SMMs, which blocks the reversal of the magnetization vector. Such an exhibition has potential applications in information storage and spintronics at the molecular level.[2,12] The inherence of the lanthanide ions' large anisotropy (e.g., Dy^{III} and Tb^{III}) could serve to generate SMMs with considerable effective barrier. By replacement of the isotropic lanthanide ion (e.g., Gd^{III}) by the anisotropic one, the large-spin nanomagnets with large magnetic anisotropy could result in SMM behavior.

Received: October 27, 2012
Published: December 24, 2012

   dx.doi.org/10.1021/ic302349f | Inorg. Chem. 2013, 52, 457−463

Herein, we report four 3d−4f clusters (Figures 1 and S1 in the Supporting Information, SI), $[Ln_6Mn_{12}O_7(OH)_{10}(OAc)_{14}(mpea)_8]$·solv (Ln = Gd, solv = $13H_2O$·6MeOH, **1-Gd**; Ln = Tb, solv = $13H_2O$·7MeOH, **1-Tb**) and $[Ln_6Mn_{12}O_9(OH)_8(OAc)_{10}(mpea)_8(mp)_2(MeOH)_2(H_2O)_2]$·solv (Ln = Gd, solv = $17H_2O$·12MeOH, **2-Gd**; Ln = Tb, solv = $26H_2O$·2MeOH, **2-Tb**), where Hmp = 2-hydroxy-5-methylisophthalaldehyde and H_2mpea = 2-hydroxy-3-[[(2-hydroxyethyl)imino]methyl]-5-methylbenzaldehyde (Scheme 1), with symmetry-related

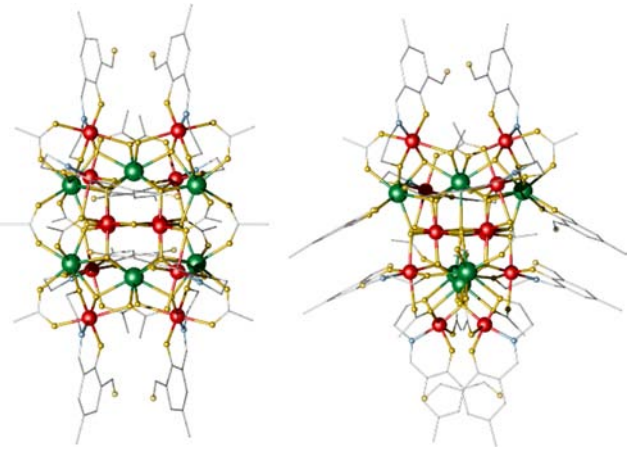

Figure 1. Molecular structures of **1** (left) and **2** (right). Color code: green, Ln^{III}; red, Mn^{III}; yellow, O; blue, N; gray, C. Hydrogen atoms and lattice solvent molecules have been omitted for clarity.

Scheme 1. Ligands of Hmp and H_2mpea

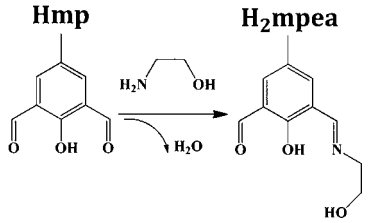

$[Ln^{III}_6Mn^{III}_{12}]$ cores, and the assignments of the solvents were based on elemental analysis by minimization of the residuals. Although they are dominantly ferromagnetic and possess huge magnetic moments, which are helpful for enhancing the effective barriers and magnetic entropy changes, the ground states are varied because of the different orientations of the linear $\{Ln^{III}_3\}$ units and the Jahn−Teller axes of Mn^{III} ions of the $\{Mn^{III}_8O_{13}\}$ unit. The distinct ground states of the symmetry-related cores could significantly change the magnetic properties, such as the magnetic entropies and effective barriers. In this way, they are the analogues of our previously reported $[Dy^{III}_6Mn^{III}_{12}]$ SMMs (**1-Dy** and **2-Dy**) and $[Y^{III}_6Mn^{III}_{12}]$ cluster (**2-Y**).[9a]

EXPERIMENTAL SECTION

Materials and General Procedures. All of the chemicals were obtained from commercial sources and used without further purification. The carbon, hydrogen, and nitrogen microanalyses were carried out with an Elementar Vario-EL CHNS elemental analyzer. The Fourier transform infrared (FT-IR) spectra were recorded from KBr pellets in the range 4000−400 cm^{-1} with a Bruker EQUINOX 55 FT-IR spectrometer. X-ray Powder diffraction (XRPD) intensities for polycrystalline samples were measured at room temperature on a Bruker D8 Advance diffractometer (Cu Kα, λ = 1.54056 Å) by scanning over the range 4−50° with step 0.2°/s. The calculated patterns were generated with Mercury.

Synthesis. *Synthesis of* ***1-Ln***. A mixture of 2-hydroxy-5-methylisophthalaldehyde (33 mg, 0.2 mmol) and 2-aminoethanol (15 mg, 0.25 mmol) in methyl cyanide (MeCN)/methanol (MeOH) (8/8 mL) was stirred and heated at 80 °C for 1 h, and the solution turned dark yellow. Then $LnCl_3·6H_2O$ (Ln = Gd, Tb; 37 mg, 0.1 mmol), $Mn(OAc)_2·4H_2O$ (49 mg, 0.2 mmol), and triethylamine (30 mg, 0.3 mmol) were added in order. The resulting brown solution was stirred under ambient conditions for another 2 h and then filtered. Small black crystals of **1-Ln** (~6% yield) were obtained until the solution nearly dried. Elem anal. Calcd for **1-Gd** (4779.60): C, 30.66; H, 4.01; N, 2.34. Found: C, 29.77; H, 4.07; N, 2.32. IR (KBr disk, cm^{-1}): 3434s, 2926m, 2866m, 1677s, 1634vs, 1549vs, 1447vs, 1323m, 1292m, 1232m, 1166m, 1050m, 973w, 867w, 835w, 766w, 617s, 541s. Elem anal. Calcd for **1-Tb** (4821.66): C, 30.64; H, 4.06; N, 2.32. Found: C, 30.58; H, 3.99; N, 2.46. IR (KBr disk, cm^{-1}): 3424s, 2927nm, 2866m, 1677s, 1635vs, 1548vs, 1447vs, 1322m, 1290m, 1231m, 1166m, 1050w, 973w, 867w, 835w, 745w, 618s, 541s.

Synthesis of ***2-Ln***. 2-Hydroxy-5-methylisophthalaldehyde (33 mg, 0.2 mmol) and 2-aminoethanol (12 mg, 0.2 mmol) in MeCN/MeOH (8/8 mL) were mixed at room temperature. Then $GdCl_3·6H_2O$ (37 mg, 0.1 mmol), $Mn(OAc)_2·4H_2O$ (49 mg, 0.2 mmol), and triethylamine (30 mg, 0.3 mmol) were immediately added in order. The resulting brown solution was stirred under ambient conditions for another 2 h and then filtered. Black prism crystals of **2-Ln** (~6% yield) were obtained until the solution nearly dried. Elem anal. Calcd for **2-Gd** (5232.13): C, 32.14; H, 4.51; N, 2.14. Found: C, 31.59; H, 4.83; N, 2.39. IR (KBr disk, cm^{-1}): 3421s, 2924m, 2866m, 1677s, 1636s, 1549vs, 1448vs, 1418vs, 1322m, 1290m, 1231s, 1047m, 971m, 635s, 559s. Elem anal. Calcd for **2-Tb** (5065.86): C, 30.82; H, 4.18; N, 2.21. Found: C, 30.74; H, 4.20; N, 2.24. IR (KBr disk, cm^{-1}): 3428s, 2924m, 2866m, 1677s, 1636s, 1549vs, 1447vs, 1419vs, 1322m, 1291m, 1231s, 1046m, 970m, 636s, 559s.

X-ray Structure Determination. The intensity data were recorded on a Rigaku R-AXIS SPIDE IP system with Mo Kα radiation. The structure was solved by direct methods, and all non-hydrogen atoms were refined anisotropically by least squares on F^2 using the *SHELXTL* program. Hydrogen atoms on organic ligands were generated by the riding model (Sheldrick, G. M. *SHELXTL97, Program for crystal structure refinement*, University of Göttingen: Göttingen, Germany, 1997).[13a] The disordered water and methanol molecules could not be modeled properly; thus, the program *SQUEEZE*,[13b] a part of the *PLATON* package of crystallographic software, was used to calculate the solvent disorder area and remove its contribution to the overall intensity data. CCDC 832665−832666 and 903377−903378 contain the supplementary crystallographic data for this paper. These data can be obtained free of charge via www.ccdc.cam.ac.uk/conts/retrieving.html (or from the Cambridge Crystallographic Data Centre, 12 Union Road, Cambridge CB21EZ, U.K.; fax (+44)1223-336-033 or e-mail deposit@ccdc.cam.ac.uk).

Magnetic Measurements. Magnetic susceptibility measurements were performed using a Quantum Design MPMS XL-7 SQUID magnetometer. Diamagnetism was estimated from Pascal constants.

RESULTS AND DISCUSSION

Structural Analysis. The $[Ln^{III}_6Mn^{III}_{12}]$ molecules possess D_2 site symmetry (high symmetry) in **1-Ln** and C_1 symmetry (low symmetry) in **2-Ln** (Figures 1 and 2). All of the metal ions are examined to be trivalent by bond-valence-sum (BVS) calculations (Tables 1 and S1 in the SI).[14]

All mpea ligands act in μ-η^3:η^1-chelating−bridging mode through the alkoxy bridges, while each mp ligand is chelating a single Ln^{III} ion. **1-Ln** contains seven μ_4-O (one of which is in square geometry while others are tetrahedra), eight μ_3-OH, two μ-OH, eight μ_3-η^1:η^1:η^1-OAc, and six μ-η^1:η^1-OAc as bridges. Four Ln^{III} ions in the corner for **1-Ln** are eight-coordinate

dx.doi.org/10.1021/ic302349f | Inorg. Chem. 2013, 52, 457−463

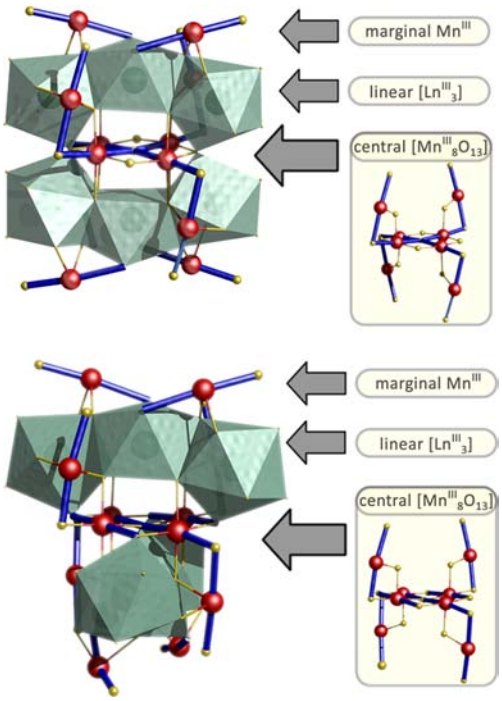

Figure 2. Polyhedral representations of **1-Ln** (top) and **2-Ln** (bottom). Each Ln^{III} is highlighted as a green polyhedron, and the Jahn–Teller axes of Mn^{III} ions are highlighted as thick and blue sticks. Color code: green, Ln^{III}; red, Mn^{III}; yellow, O.

(square antiprism), while the other two are nine-coordinate (capped square antiprism). Complex **2-Ln** contains one pyramidal μ_5-O, two tetrahedral μ_4-O, six μ_3-O, eight μ_3-OH, two μ-OH, six μ_3-η^1:η^1:η^1-OAc, and four μ-η^1:η^1-OAc as bridges. The coordination spheres of **2-Ln** are eight-coordinate (square antiprism and biaugmented trigonal prism) and nine-coordinate (capped square antiprism) for the two $\{Ln^{III}_3\}$ units, respectively. Ln···Ln distances (3.73 Å for both **1-Gd** and **1-Tb**, 3.75–3.80 Å for **2-Gd**, and 3.72–3.76 Å for **2-Tb**) in the $\{Ln^{III}_3\}$ units and Ln···Ln···Ln angles (155.7° for **1-Gd**, 155.6° for **1-Tb**, 159.7° and 161.8° for **2-Gd**, and 159.7° and 162.4° for **2-Tb**) in $\{Ln^{III}_3\}$ units are similar to those for the previously reported ferromagnetic $[Ln^{III}_3]$ complexes.[9k]

The cores can be described as composed by several analogical building units (Figure 2): (A) the marginal Mn^{III} ions; (B) the linear $\{Ln^{III}_3\}$ units; (C) the central $\{Mn^{III}_8O_{13}\}$ unit, assembling like ABCBA. One of the noteworthy differences of the two clusters is the orientation of the two related $\{Ln^{III}_3\}$ units. They are nearly parallel (~11°) and perpendicular (~83°) to one another in **1-Ln** and **2-Ln**, respectively. As a result, the Jahn–Teller axes of Mn^{III} in the $\{Mn^{III}_4O_5\}$ tetragon of the central $\{Mn^{III}_8O_{12}\}$ unit are intersecting for **1-Ln** but parallel for **2-Ln**. The different orientations of the Jahn–Teller axes in the $\{Mn^{III}_4O_5\}$ tetragons (Figure 2) reflect the distinct interactions of the magnetic orbitals for the two compounds. The two clusters are likely to exhibit different magnetic behaviors.

Magnetic Properties. The direct-current (dc) magnetic susceptibility data were collected in the temperature range 2–290 K (Figure 3). At room temperature, the $\chi_M T$ values are 85.5, 109.4, 81.5, and 104.8 cm^3 K mol^{-1} for **1-Gd**, **1-Tb**, **2-Gd**, and **2-Tb**, respectively, which are close to the expected values for the uncoupled $[Ln^{III}_6Mn^{III}_{12}]$ cores (Mn^{III}, $S = 2$, $g = 2$; Gd^{III}, $S = {}^7/_2$, $L = 0$, $^8S_{7/2}$, $g = 2$; Tb^{III}, $S = 3$, $L = 3$, $^7F_6$, $g = {}^3/_2$; 83.3 cm^3 K mol^{-1} for Gd species and 106.9 cm^3 K mol^{-1} for Tb species).[15] Upon lowering of the temperature, the $\chi_M T$ products of **1-Ln** stay nearly constant and then sharply increase to a maximum (254.7 cm^3 K mol^{-1} for **1-Gd** and 320.8 cm^3 K mol^{-1} for **1-Tb**) at 3.5 K, indicating dominant ferromagnetic interactions, and then decrease because of the zero-field splitting (ZFS) of Mn^{III} ions and/or crystal-field effect of Tb^{III} and/or intermolecular antiferromagnetic interactions. For **2**, the $\chi_M T$ products decrease first, then respectively increase to 115.6 cm^3 K mol^{-1} at 4 K for **2-Gd** and 98.8 cm^3 K mol^{-1} at 6.5 K for **2-Tb**, and then decrease again. The susceptibility data obey the Curie–Weiss law with $C = 84.0$ (1) cm^3 K mol^{-1} and $\theta = 8.0(2)$ K for **1-Gd**, $C = 107.7(2)$ cm^3 K mol^{-1} and $\theta = 4.0(4)$ K for **1-Tb**, $C = 82.5(4)$ cm^3 K mol^{-1} and $\theta = -6.5(9)$ K for **2-Gd**, and $C = 106.9(2)$ cm^3 K mol^{-1} and $\theta = -6.8(3)$ K for **2-Tb** (from 290 to 50 K; Figure S1 in the SI), respectively.

To further investigate the interactions of Ln···Ln and Ln···Mn in **2-Ln**, especially the Gd species, we subtract the

Table 1. Crystal Data and Structure Refinements for $[Ln^{III}_6Mn^{III}_{12}]$ Complexes

	1-Gd	1-Tb	2-Gd	2-Tb
formula	$C_{122}H_{190}N_8Mn_{12}Gd_6O_{88}$	$C_{123}H_{194}N_8Mn_{12}Tb_6O_{89}$	$C_{140}H_{234}N_8Mn_{12}Gd_6O_{100}$	$C_{130}H_{210}N_8Mn_{12}Tb_6O_{98}$
M/g mol^{-1}	4779.60	4821.66	5232.13	5065.86
cryst syst	orthorhombic	orthorhombic	triclinic	triclinic
space group	*Fddd*	*Fddd*	$P\bar{1}$	$P\bar{1}$
a/Å	22.6535(17)	22.8370(7)	19.5839(11)	19.6524(6)
b/Å	37.360(3)	37.3301(12)	20.1363(10)	21.3716(7)
c/Å	46.159(3)	46.1780(15)	26.3657(12)	26.7943(9)
α/deg	90	90	81.921(1)	95.474(1)
β/deg	90	90	89.758(1)	98.128(1)
γ/deg	90	90	66.470(1)	115.139(1)
V/Å^3	39066(5)	39367(2)	9422.7(8)	9932.5(6)
Z	8	8	2	2
reflns collected	31137	29294	56179	72661
unique reflns	9330	9439	30386	41332
R1[a] [$I > 2\sigma(I)$]	0.0644	0.0620	0.1066	0.0679
wR2[b] (all data)	0.1980	0.1577	0.3259	0.1909

[a] $R1 = \sum||F_o| - |F_c||/\sum|F_o|$. [b] $wR2 = [\sum w(F_o^2 - F_c^2)^2/\sum w(F_o^2)^2]^{1/2}$.

dx.doi.org/10.1021/ic302349f | *Inorg. Chem.* 2013, 52, 457–463

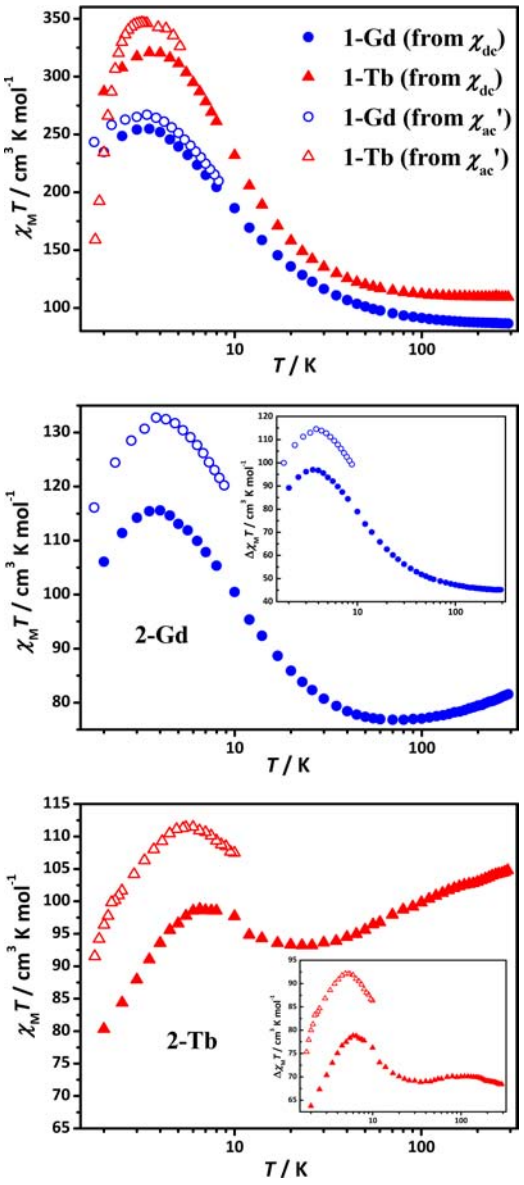

Figure 3. Temperature dependence of the $\chi_M T$ products in the temperature range of 300−2 K for **1-Gd** and **1-Tb** (top), **2-Gd** (middle), and **2-Tb** (bottom). Inset: $\chi_M T$ versus T plots of subtraction of that of **2-Y** from the plot of **2-Gd** and **2-Tb**. The solid symbols are from dc susceptibilities (H_{dc} = 500 Oe), and the empty ones are from ac in-phase susceptibilities (H_{dc} = 0 Oe; H_{ac} = 5 Oe).

plot of **2-Y** from the plot of **2-Gd** and **2-Tb** (inset of Figure 3). Upon cooling, the $\Delta\chi_M T$ values overall increase to a maximum, suggesting the presence of ferromagnetic interaction of Ln···Ln.

In order to clarify the spin ground states for **1-Gd** and **2-Gd** in the absence of an external field, $\chi_M{}'T$ alternating-current (ac) data under zero dc field and their subtracted ones are also illustrated in Figure 3. It is worth noting that the deviations between dc and ac susceptibilities should attribute to the difference between the applied fields, altering the population of ground states and the low-lying excited states. Just like [Mn_{19}] with a $S = {}^{83}/_{2}$ ground state, M versus H is nonlinear upon exceeding an applied field that is not too high indeed (300 Oe),[5] resulting in smaller susceptibilities ($\chi_{dc} = M/H$) even in a small dc field.

The maximum (114.6 cm^3 K mol^{-1}) of $\Delta\chi_M{}'T$ for **2-Gd** indicates that the {$Gd^{III}{}_3$} unit is ferromagnetically coupled (two {$Gd^{III}{}_3$} units, $S = {}^{21}/_{2}$, 2 × 60.4 = 120.8 cm^3 K mol^{-1}). According to $\chi_M{}'T$ data and the molecular structures, the possible spin ground states are respectively S_T = 23 for **1-Gd** and S_T = 16 for **2-Gd** (Scheme 2) with ferromagnetic Gd···Gd

Scheme 2. Spin Arrangement of 1-Gd and 2-Gd[a]

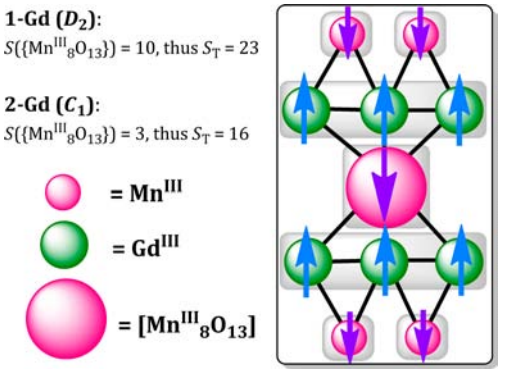

[a]Mn···Gd interactions: antiferromagnetic. Gd···Gd interactions: ferromagnetic.

interactions and antiferromagnetic Gd···Mn interactions, whose expected values (276 cm^3 K mol^{-1} for **1-Gd** and 136 cm^3 K mol^{-1} for **2-Gd**) are in agreement with the maxima of the $\chi_M{}'T$ values (266.9 cm^3 K mol^{-1} for **1-Gd** and 132.7 cm^3 K mol^{-1} for **2-Gd**). The central {$Mn^{III}{}_8O_{13}$} cores are dominantly ferromagnetically coupled for **1-Gd** (S = 10) and dominantly antiferromagnetically coupled for **2-Gd** (S = 3). It may originate from the distinct interactions of the magnetic orbitals for their different orientations of the Jahn−Teller axes. The spins of the central {$Mn^{III}{}_8O_{13}$} units are consistent with the analogous nanomagnets of **2-Dy** and **2-Y**.[9a]

The nonoverlapping of isofields in the reduced magnetization ($M/N\beta$) versus H/T plots (Figure 4) unambiguously indicate the presence of significant magnetic anisotropy. Thus, if considering the ZFS on Mn^{III} ions and thermal population of low-lying spin excited states arising from the usually weak Gd···Mn interactions, it is reasonable that the maxima are slightly smaller than the expected values. The low-temperature reduced magnetization for **1-Gd** and **2-Gd** approaches 77 and 69 $N\beta$ at 7 T, respectively. The values are in the range of the calculated values of the ground state (S_T = 23 for **1-Gd**, 46 $N\beta$; S_T = 16 for **2-Gd**, 32 $N\beta$) and the saturated ones (S_{max} = 45, 90 $N\beta$), which are due to the progressive population of the Zeeman sublevels of low-lying excited states with larger spin following with increasing magnetic fields.

The dominant ferromagnetic coupling gives rise to a large spin ground state that is favorable for enhancing the magnetic entropy at zero field, and the multiple low-lying excited states with larger spin make the magnetic entropy decrease rapidly even under a small magnetic field and in a relatively high temperature range. Furthermore, neither long-range order nor slow relaxation of magnetization was observed as the absent signals of ac susceptibilities (Figure S2 in the SI). So, we continued to evaluate the MCE for **1-Gd** and **2-Gd**.

Magnetization data can be employed for estimating the MCE parameters (magnetic entropy change, $-\Delta S_m$) by the Maxwell relation $\Delta S_m(T)_{\Delta H} = \int [\partial M(T,H)/\partial T]_H \, dH$.[4,15b] It can be seen that both of the $-\Delta S_m$ values increase gradually with increasing

dx.doi.org/10.1021/ic302349f | Inorg. Chem. 2013, 52, 457−463

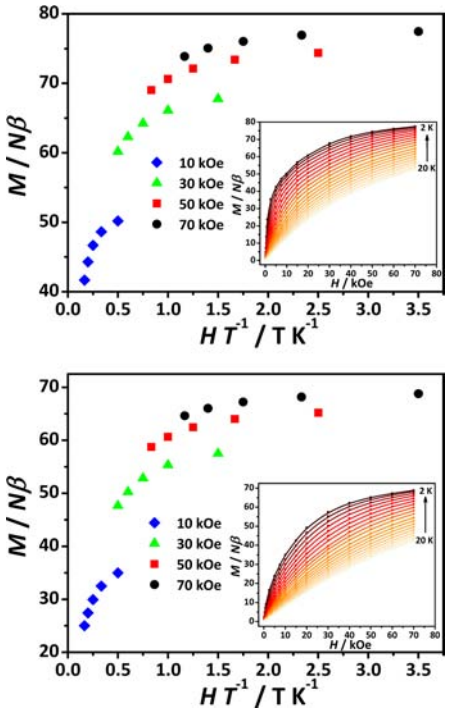

Figure 4. Plots of $M/N\beta$ versus H/T for **1-Gd** (top) and **2-Gd** (bottom) in the temperature range of 2−7 K at the indicated applied fields. Inset: $M/N\beta$ versus H in the temperature range of 2−20 K.

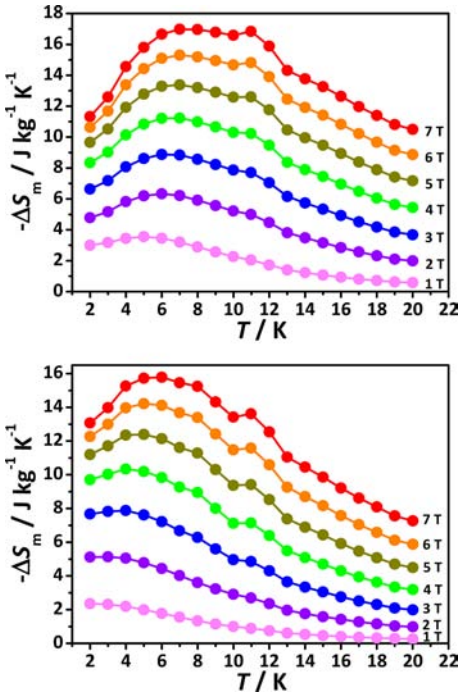

Figure 5. Experimental $-\Delta S_m$ obtained from the magnetization data of **1-Gd** (top) and **2-Gd** (bottom) at various temperatures and magnetic field changes.

ΔH and increasing temperature, reaching a maximum value of 17.0 J kg^{-1} K^{-1} at 7 K for **1-Gd** and 15.8 J kg^{-1} K^{-1} at 6 K for **2-Gd**, under a magnetic field change of 7 T (Figure 5). The magnetic entropy changes of **1-Gd** are overall larger than that of **2-Gd** because of the larger spin of the central $\{Mn^{III}_8O_{13}\}$ unit of **1-Gd** (Scheme 2).

Two extreme situations are considered: (1) The $[Gd^{III}_6Mn^{III}_{12}]$ clusters are so completely ferromagnetically coupled that only $S_{max} = 45$ is populated. So, the possible maxima of the magnetic entropy can be calculated by $R\ln(2S_{max} + 1)$, which are respectively 7.75 and 7.17 J kg^{-1} K^{-1} for **1-Gd** and **2-Gd**. (2) The clusters are fully decoupled. Therefore, it should be rewritten as $R[n_{Gd}\ln(2S_{Gd} + 1) + n_{Mn}\ln(2S_{Mn} + 1)]$, which is respectively 54.6 and 50.5 J kg^{-1} K^{-1} for **1-Gd** and **2-Gd**. It is apparent that the experimental $-\Delta S_m$ are between these two extreme situations because of the existence of magnetic exchanges and magnetic anisotropies that remove the degeneracies of multiple spin states.

To our knowledge, the cusp of the magnetic entropy change for all pure Gd^{III}-based coordination complexes is situated at low temperature (~2 K) and rapidly decreases upon heating or cooling.[16] In this work, the maxima shift to 6 K for **2-Gd** and 7 K for **1-Gd**, which originate from the magnetic exchange and magnetic anisotropy that split the spin multiples. It is worth mentioning that their $-\Delta S_m$ are among the highest reported magnetic refrigerants in such a high-temperature range of 6−20 K especially under a small magnetic field change. Only a small amount of 3d−4f complexes reported the magnetic entropy changes up to 20 K. In $[Gd_{42}M_{10}]$ (M = Co and Ni), $-\Delta S_m$ obtained from the heat capacity, although reaching very large values, positively deviate from that from magnetization in the high temperature range.[6h] In the $[\{Gd(OAc)_3(H_2O)_2\}_2]\cdot 4H_2O$ cluster with remarkable MCE, $-\Delta S_m$ are ~20 J kg^{-1} K^{-1} at 10 K and ~10 J kg^{-1} K^{-1} at 20 K under 7 T and <1 J kg^{-1} K^{-1} at 10−20 K under 1 T, which are smaller than those of this work at high temperatures and under lower fields.[16a]

It is well-known that a positive D value favors $M_S = 0$ while a negative one favors $M_S = \pm S$ states. Molecules with negative ZFS parameters actually result in larger MCE at high temperature and under small magnetic field because of its rapidly decreasing S_m upon demagnetization. However, it is not the case for **1-Ln** and **2-Ln** because of the absence of out-of-phase ac signals, suggesting $D > 0$ arose by Mn^{III} ions. As for magnetic exchange, ferromagnetic interaction favors larger spins, leading to large S_m ($H = 0$) and also causing more rapid decreases following a decreasing magnetic field. Thus, it is ferromagnetic interaction that enlarges MCE for **1-Ln** and **2-Ln** at high temperatures and under low fields. That is to say, that although ferromagnetic interaction tends to limit the performance in the low-temperature range, it reasonably favors relatively larger MCE in the high-temperature range, causing it to decrease very slowly upon increasing temperatures. It helps to stabilize $-\Delta S_m$ in a wide temperature range (FWHM of their $-\Delta S_m$ are >18 K), maximizing the refrigerant capacity[17] and avoiding excessive fluctuation. These two 3d−4f complexes are likely to be good candicates for their relatively large MCE and very broad temperature span because their ferromagnetic interactions.

The large intrinsic anisotropy of the Tb^{III} ion makes **1-Tb** and **2-Tb** exhibit strong frequency-dependent out-of-phase ac signals (Figures 6 and S3), which is indicative of slow relaxation of magnetization associated with SMM-like behavior. For an absence of out-of-phase signals for **2-Y**, the SMM-like behavior may come from Tb^{III} ions. The nonoverlapping $M-H/T$ plots also suggest the presence of strong magnetic anisotropies (Figure 7).

The Cole−Cole plots show quasi-semicircles and are fitted by the generalized Debye model (Figure S4 in the SI; α = 0.46−0.47 for **1-Tb** and α = 0.44−0.49 for **2-Tb**),[18] indicating

dx.doi.org/10.1021/ic302349f | Inorg. Chem. 2013, 52, 457−463

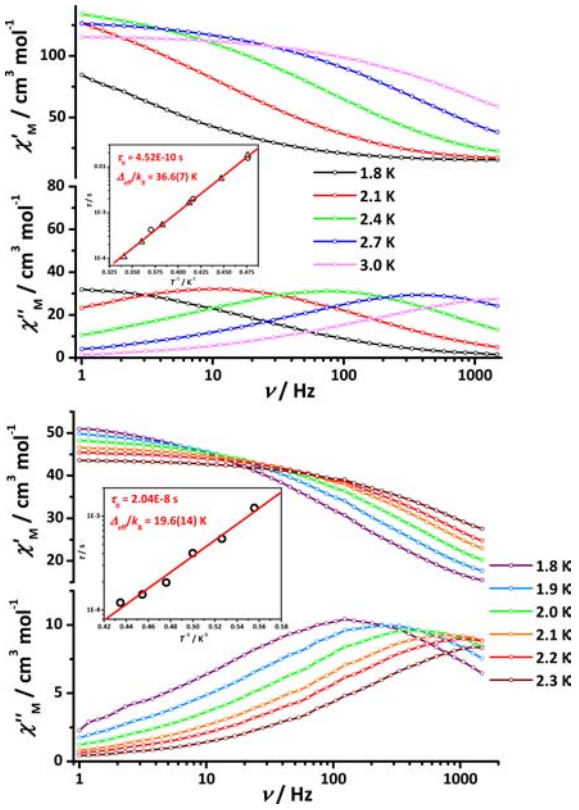

Figure 6. Plots of ac susceptibility versus temperature for **1-Tb** (top) and **2-Tb** (bottom) oscillating at 1−1488 Hz at H_{ac} = 5 Oe and H_{dc} = 0. Inset: τ versus T^{-1} plots obtained from $\chi_M''(T)$ (Δ) and $\chi_M''(\nu)$ (○). The solid lines correspond to the Arrhenius law for **1-Tb** (top) and **2-Tb** (bottom).

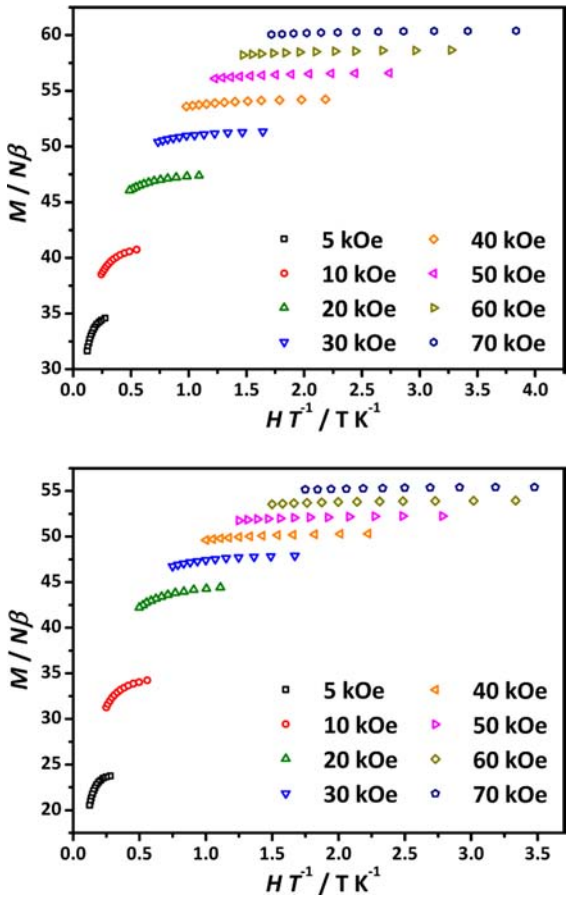

Figure 7. Plots of $M/N\beta$ versus H/T for **1-Tb** (top) and **2-Tb** (bottom) in the temperature range of 1.8−4 K at the indicated applied fields.

the presence of a moderate distribution of slow relaxation. The φ values $\{\varphi = \Delta T_P/[T_P\Delta(\log f)]\}$ of 0.13 (**1-Tb**) and 0.19 (**2-Tb**) suggest a superparamagnetic-like behavior instead of a spin-glass one (φ < 0.1; Figure S5 in the SI).[19] The effective barrier, Δ_{eff}, can be obtained by the Arrhenius law from the relaxation time, giving Δ_{eff}/k_B = 36.6(7) K (preexponential factor $\tau_0 = 4.52 \times 10^{-10}$ s) for **1-Tb** and Δ_{eff}/k_B = 19.6(14) K ($\tau_0 = 2.04 \times 10^{-8}$ s) for **2-Tb**, respectively (inset of Figure 6). Both of their effective energy barriers are slightly larger than the Dy^{III} analogues (35.1 K for **1-Dy** and 18.2 K for **2-Dy**), and it is the third largest in the families of Mn−Ln SMMs.[9f,g] The high-symmetry $[Tb^{III}_6Mn^{III}_{12}]$ possesses larger magnetic moments and higher effective barriers and vice versa. Here again it implies the important roles in the magnetic dynamics of the ground state and the molecular symmetry of this $[Ln^{III}_6Mn^{III}_{12}]$ family, originating from the difference of the orientation of the $\{Ln^{III}_3\}$ units (parallel and perpendicular) and the Jahn−Teller axes of Mn^{III} in the $\{Mn^{III}_8O_{13}\}$ units.

CONCLUSION

In this study, we have generated four nanomagnets with $[Ln^{III}_6Mn^{III}_{12}]$ cores. They all possess huge magnetic moments and dominant ferromagnetic interactions. For the Gd ones, cryogenic MCE investigations illustrate that the magnetic entropy changes are stable in quite a broad temperature span compared with other molecular magnetic refrigerants and are among the highest reported ones in the temperature range of 6−20 K, especially under a small magnetic field change. For the Tb ones, both of them exhibit SMM behavior with considerable energy barriers in the families of 3d−4f SMMs. It is found that the spin ground state and the magnetic entropy change of the high-symmetrical **1-Gd** (S = 23, $-\Delta S_m$ = 17.0 J kg^{-1} K^{-1}) is larger than the lower one, **2-Gd** (S = 16, $-\Delta S_m$ = 15.8 J kg^{-1} K^{-1}), and the effective barrier of the high-symmertrcal **1-Tb** (36.6 K) is higher than the lower one, **2-Tb** (19.6 K). Therefore, we further confirm that the different symmetries of these clusters can result in distinct magnetic characters, such as spin ground state, magnetic entropy, magnetic anisotropy, and slow relaxation of magnetization.

ASSOCIATED CONTENT

Supporting Information

X-ray crystallographic data in CIF format, magnetic data, and BVS calculations. This material is available free of charge via the Internet at http://pubs.acs.org.

AUTHOR INFORMATION

Corresponding Author

*E-mail: tongml@mail.sysu.edu.cn.

Notes

The authors declare no competing financial interest.

ACKNOWLEDGMENTS

This work was supported by the "973 Project" (2012CB821704), the NSFC (Grants 91122032, 90922009, 21121061, and J1103305), and a Foundation for the Author of

National Excellent Doctoral Dissertation of the People's Republic of China (Grant 20100171110015).

REFERENCES

(1) (a) Aromí, G.; Brechin, E. K. *Synthesis of 3d Metallic Single-Molecule Magnets*; Springer: Berlin, 2006; Vol. *122*, p 1. (b) Sessoli, R.; Powell, A. K. *Coord. Chem. Rev.* **2009**, *253*, 2328.

(2) (a) Gatteschi, D.; Sessoli, R.; Villain, J. *Molecular Nanomagnets*; Oxford University Press: New York, 2006. (b) Domingo, N.; Bellido, E.; Ruiz-Molina, D. *Chem. Soc. Rev.* **2012**, *41*, 258. (c) Troiani, F.; Affronte, M. *Chem. Soc. Rev.* **2011**, *40*, 3119. (d) Dei, A.; Gatteschi, D. *Angew. Chem., Int. Ed.* **2011**, *50*, 11852. (e) Jiang, S. D.; Goβ; Cervetti, C.; Bogani, L. *Sci. China Chem.* **2012**, *55*, 867. (f) Cornia, A.; Mannini, M.; Sainctavit, P.; Sessoli, R. *Chem. Soc. Rev.* **2011**, *40*, 3076. (g) Gatteschi, D.; Sessoli, R. *Angew. Chem., Int. Ed.* **2003**, *42*, 268.

(3) (a) Fenske, D.; Ohmer, J.; Hachgenei, J. *Angew. Chem., Int. Ed. Engl.* **1985**, *24*, 993. (b) Liu, T.; Zhang, Y. J.; Wang, Z. M.; Gao, S. *J. Am. Chem. Soc.* **2008**, *130*, 10500. (c) Alborés, P.; Rentschler, E. *Angew. Chem., Int. Ed.* **2009**, *48*, 9366. (d) Gatteschi, D.; Fittipaldi, M.; Sangregorio, C.; Sorace, L. *Angew. Chem., Int. Ed.* **2012**, *51*, 4792.

(4) (a) Spichkin, Y. I.; Zvezdin, A. K.; Gubin, S. P.; Mischenko, A. S.; Tishin, A. M. *J. Phys. D: Appl. Phys.* **2001**, *34*, 1162. (b) Evangelisti, M.; Luis, F.; de Jongh, L. J.; Affronte, M. *J. Mater. Chem.* **2006**, *16*, 2534. (c) Evangelisti, M.; Candini, A.; Ghirri, A.; Affronte, M.; Brechin, E. K.; McInnes, E. J. L. *Appl. Phys. Lett.* **2005**, *87*, 072504. (d) Evangelisti, M.; Brechin, E. K. *Dalton Trans.* **2010**, *39*, 4672. (e) Evangelisti, M.; Candini, A.; Affronte, M.; Pasca, E.; de Jongh, L. J.; Scott, R. T. W.; Brechin, E. K. *Phys. Rev. B* **2009**, *79*, 104414. (f) Sessoli, R. *Angew. Chem., Int. Ed.* **2011**, *51*, 43.

(5) Ako, A. M.; Hewitt, I. J.; Mereacre, V.; Clérac, R.; Wernsdorfer, W.; Anson, C. E.; Powell, A. K. *Angew. Chem., Int. Ed.* **2006**, *45*, 4926.

(6) (a) Zheng, Y.-Z.; Evangelisti, M.; Tuna, F.; Winpenny, R. E. P. *J. Am. Chem. Soc.* **2012**, *134*, 1057. (b) Long, L.-S.; Huang, R.-B.; Zheng, L.-S.; Zheng, Z.-P. *Angew. Chem., Int. Ed.* **2011**, *50*, 10649. (c) Liu, J.-L.; Leng, J.-D.; Lin, Z.; Tong, M.-L. *Chem.—Asian J.* **2011**, *6*, 1007. (d) Hosoi, A.; Yukawa, Y.; Igarashi, S.; Teat, S. J.; Roubeau, O.; Evangelisti, M.; Cremades, E.; Ruiz, E.; Barrios, L. A.; Aromí, G. *Chem.—Eur. J.* **2011**, *17*, 8264. (e) Manoli, M.; Johnstone, R. D. L.; Parsons, S.; Murrie, M.; Affronte, M.; Evangelisti, M.; Brechin, E. K. *Angew. Chem., Int. Ed.* **2007**, *46*, 4456. (f) Langley, S. K.; Chilton, N. F.; Moubaraki, B.; Hooper, T.; Brechin, E. K.; Evangelisti, M.; Murray, K. S. *Chem. Sci.* **2011**, *2*, 1166. (g) Karotsis, G.; Kennedy, S.; Teat, S. J.; Beavers, C. M.; Fowler, D. A.; Morales, J. J.; Evangelisti, M.; Dalgarno, S. J.; Brechin, E. K. *J. Am. Chem. Soc.* **2010**, *132*, 12983. (h) Peng, J.-B.; Zhang, Q.-C.; Kong, X.-J.; Zheng, Y.-Z.; Ren, Y.-P.; Long, L.-S.; Huang, R.-B.; Zheng, L.-S.; Zheng, Z. *J. Am. Chem. Soc.* **2012**, *134*, 3314.

(7) (a) Sharples, J. W.; Zheng, Y.-Z.; Tuna, F.; Mclnnes, E. J. L.; Collison, D. *Chem. Commun.* **2011**, *47*, 7650. (b) Leng, J.-D.; Liu, J.-L.; Tong, M.-L. *Chem. Commun.* **2012**, *48*, 5286. (c) Leng, J.-D.; Liu, J.-L.; Zheng, Y.-Z.; Ungur, L.; Chibotaru, L. F.; Guo, F.-S.; Tong, M.-L. *Chem. Commun.* **2013**, *49*, 158.

(8) (a) Sessoli, R.; Tsai, H.-L.; Schake, A. R.; Wang, S.; Vincent, J. B.; Folting, K.; Gatteschi, D.; Christou, G.; Hendrickson, D. N. *J. Am. Chem. Soc.* **1993**, *115*, 1804. (b) Sessoli, R.; Gatteschi, D.; Caneschi, A.; Novak, M. A. *Nature* **1993**, *365*, 141.

(9) (a) Liu, J.-L.; Guo, F.-S.; Meng, Z.-S.; Zheng, Y.-Z.; Leng, J.-D.; Tong, M.-L.; Ungur, L.; Chibotaru, L. F.; Heroux, K. J.; Hendrickson, D. N. *Chem. Sci.* **2011**, *2*, 1268. (b) Stamatatos, T. C.; Abboud, K. A.; Wernsdorfer, W.; Christou, G. *Angew. Chem., Int. Ed.* **2007**, *46*, 884. (c) Baskar, V.; Gopal, K.; Helliwell, M.; Tuna, F.; Wernsdorfer, W.; Winpenny, R. E. P. *Dalton Trans.* **2010**, *39*, 4747. (d) Moushi, E. E.; Stamatatos, T. C.; Wernsdorfer, W.; Nastopoulos, V.; Christou, G.; Tasiopoulos, A. J. *Inorg. Chem.* **2009**, *48*, 5049. (e) Ako, A. M.; Mereacre, V.; Clerac, R.; Hewitt, I. J.; Lan, Y.; Buth, G.; Anson, C. E.; Powell, A. K. *Inorg. Chem.* **2009**, *48*, 6713. (f) Papatriantafyllopoulou, C.; Wernsdorfer, W.; Abboud, K. A.; Christou, G. *Inorg. Chem.* **2011**, *50*, 421. (g) Mereacre, V.; Ako, A. M.; Clérac, R.; Wernsdorfer, W.; Hewitt, I. J.; Anson, C. E.; Powell, A. K. *Chem.—Eur. J.* **2008**, *14*, 3577. (h) Stamatatos, T. C.; Teat, S. J.; Wernsdorfer, W.; Christou, G. *Angew. Chem., Int. Ed.* **2009**, *48*, 521. (i) Wang, W.-G.; Zhou, A.-J.; Zhang, W.-X.; Tong, M.-L.; Chen, X.-M.; Nakano, M.; Beedle, C. C.; Hendrickson, D. N. *J. Am. Chem. Soc.* **2007**, *129*, 1014. (j) Mondal, K. C.; Sundt, A.; Lan, Y.; Kostakis, G. E.; Waldmann, O.; Ungur, L.; Chibotaru, L. F.; Anson, C. E.; Powell, A. K. *Angew. Chem., Int. Ed.* **2012**, *51*, 7550. (k) Guo, F.-S.; Liu, J.-L.; Leng, J.-D.; Meng, Z.-S.; Lin, Z.-J.; Tong, M.-L.; Gao, S.; Ungur, L.; Chibotaru, L. F. *Chem.—Eur. J.* **2011**, *17*, 2458. (l) Guo, P.-H.; Liu, J.-L.; Zhang, Z.-M.; Ungur, L.; Chibotaru, L. F.; Leng, J.-D.; Guo, F.-S.; Tong, M.-L. *Inorg. Chem.* **2012**, *51*, 1233. (m) Liu, J.-L.; Yuan, K.; Leng, J.-D.; Ungur, L.; Wernsdorfer, W.; Guo, F.-S.; Chibotaru, L. F.; Tong, M.-L. *Inorg. Chem.* **2012**, *51*, 8538. (n) Guo, P.-H.; Liao, X.-F.; Leng, J.-D.; Tong, M.-L. *Acta Chim. Sin.* **2013**, *71*, DOI: 10.6023/A12110865. (o) Zeng, Y.-F.; Xu, G.-C.; Hu, X.; Chen, Z.; Bu, X.-H.; Gao, S.; Sañudo, E. C. *Inorg. Chem.* **2010**, *49*, 9734.

(10) (a) Warburg, E. *Ann. Phys. Chem* **1881**, *13*, 141. (b) Debye, P. *Ann. Phys.* **1926**, *81*, 1154. (c) Giauque, W. F. *J. Am. Chem. Soc.* **1927**, *49*, 1864. (d) Giauque, W. F.; McDougall, I. P. D. *Phys. Rev.* **1933**, *43*, 768.

(11) Martínez-Pérez, M.-J.; Montero, O.; Evangelisti, M.; Luis, F.; Sesé, J.; Cardona-Serra, S.; Coronado, E. *Adv. Mater.* **2012**, *24*, 4301.

(12) (a) Leuenberger, M. N.; Loss, D. *Nature* **2001**, *410*, 789. (b) Stone, R. *Science* **2009**, *325*, 1336. (c) Bogani, L.; Wernsdorfer, W. *Nat. Mater.* **2008**, *7*, 179. (d) Wernsdorfer, W.; Sessoli, R. *Science* **1999**, *284*, 133. (e) Aromí, G.; Aguilà, D.; Gamez, P.; Luis, F.; Roubeau, O. *Chem. Soc. Rev.* **2012**, *41*, 537.

(13) (a) Sheldrick, G. M. *Acta Crystallogr.* **2008**, *A64*, 112. (b) van der Sluis, P.; Spek, A. L. *Acta Crystallogr.* **1990**, *A46*, 194−201.

(14) (a) Brown, I. D.; Altermatt, D. *Acta Crystallogr., Sect. B* **1985**, *B41*, 244. (b) Liu, W.; Thorp, H. H. *Inorg. Chem.* **1993**, *32*, 4102.

(15) Kahn, O. *Molecular Magnetism*; VCH Publishers: New York, 1993. (b) Carlin, R. L. *Magnetochemistry*; Springer-Verlag: Berlin, 1986.

(16) (a) Evangelisti, M.; Roubeau, O.; Palacios, E.; Camón, A.; Hooper, T. N.; Brechin, E. K.; Alonso, J. J. *Angew. Chem., Int. Ed.* **2011**, *50*, 6606. (b) Guo, F.-S.; Leng, J.-D.; Liu, J.-L.; Meng, Z.-S.; Tong, M.-L. *Inorg. Chem.* **2012**, *51*, 405. (c) Sibille, R.; Mazet, T.; Malaman, B.; François, M. *Chem.—Eur. J.* **2012**, *18*, 12970. (d) Cremades, E.; Gomez-Coca, S.; Aravena, D.; Alvarez, S.; Ruiz, E. *J. Am. Chem. Soc.* **2012**, *134*, 10532.

(17) Wood, M. E.; Potter, W. H. *Cryogenics* **1985**, *25*, 667.

(18) Cole, K. S.; Cole, R. H. *J. Chem. Phys.* **1941**, *9*, 34.

(19) Mydosh, J. A. *Spin Glasses: An Experimental Introduction*; Taylor and Francis: London, 1993.